Supplementary Information (SI) for Nanoscale.

Solution synthesis of antiferromagnetic manganese nanoparticles

May-Line Grapotte,[a] Víctor Varela-Izquierdo,[a] Oscar Suárez-Riaño,[a] Lise-Marie Lacroix,[a]* Yann Tison,[b] Nicolas Ratel-Ramond,[a] Pier Francesco Fazzini,[c] Bruno Chaudret,[a]* Fabien Delpech.[a]*

[a] Laboratoire de Physique et Chimie des Nano-Objets (LPCNO), Université de Toulouse, CNRS, INSA, UPS, 31077 Toulouse Cedex 4, France

[b] Université de Pau et des Pays de l'Adour, E2S UPPA, CNRS, IPREM, Pau, 64000, France.

[c] CEMES CNRS UPR 8011 and Université de Toulouse, 29 rue Jeanne Marvig, BP 94347, Cedex 4, 31055 Toulouse, France

Table of Contents

1. General procedures and characterization techniques

Reagents

Diethyl ether (>99%) was purchased from Carlo Erba, toluene (>99.0%), Magnesium turnings (Mg, 99%), and 2-bromomesitylene (99%) from Alfa Aesar, $MnCl_2$ (99%), and acetonitrile (99.8 %) from Fisher Scientific, Dioxane (99.8%), Iodine (99.8%), hexadecylamine (HDA, 98%), Octadecylamine (ODA, 97%), Dodecylamine (DDA, 98%), Hexamethylendiamine (HMEDA, 99%), Tetrahydrofuran (THF, 99.5%), Cyclohexane (99.5%), Dichloromethane (99%), 1-Hexene (>99%), Phenylacetylene (98%), Acetophenone (>99%), Tetramethylethylenediamine (TMEDA, 99%), Dodecamethylenediamine (DMEDA, 98%), and palmitic acid (PA, >99%) from Sigma Aldrich, 2-butanone (>99%) from Acros Organics. All the solvents underwent a drying process using an alumina-desiccant solvent purifier and were subsequently stored inside glove box alongside with the reagents previously mentioned.

Transmissions Electron Microscopy (TEM)

The nanoparticles (NPs) were examined using transmission electron microscopy (TEM) after the deposition of a drop of a solution containing the isolated NPs in toluene over a copper grid coated with amorphous carbon. TEM analyses were conducted at the Raimond Castaing Microanalysis Centre (UAR 3623) (Toulouse, France) using a JEOL JEM 1400 electron microscope operating at 120 kV. The average size of the NPs was estimated through manual analysis of magnified micrographs measuring 200 particles on a given grid using ImageJ software.

High Resolution TEM (HR-TEM)

High-resolution transmission electron microscopy (HR-TEM) was used to examine nanoparticles (NPs) after the deposition of a drop of a solution containing the isolated NPs in toluene over an amorphous carbon-coated copper grid. The HR-TEM analysis was carried out at the Raimond Castaing Microanalysis Centre (UAR 3623) (Toulouse, France) using a JEOL cold-field emission gun (cold-FEG) JEM-ARM200F operating at 200 kV and equipped with a probe Cs corrector, achieving a spatial resolution of 0.078 nm. The samples were analyzed with the software DigitalMicrograph from Gatan.

Thermogravimetric analysis (TGA)

For our analyses, we used ATG/DSC 1 star equipment equipped with a UMX5 ultra-microbalance and a GC2000 gas exchanger. The analysis procedure is as follows:

Decomposition of organic compounds and oxidation of the sample. Initially, progressive increase in temperature from 25°C to 500°C at a speed of 10°C/min with an air flow of mL/min. Then, maintained at 500°C for 90 minutes at a flow rate of 50.0 mL/min and cooling from 500°C to 25°C at a rate of 20°C/min under an air flow of 50.0 mL/min.

Sample reduction: First, the temperature is increased from 25°C to 700°C at 30°C/min under a flow of H_2 Ar mixture (4%/96%) at 50.0 mL/min and maintained at 700°C for 90 minutes under the same gas mixture flow rate of 50.0 mL/min

From this analysis, the metal content determined by the mass ratio between the measured mass and after the analysis.

Attenuated Total Reflection Fourier Transform Infrared Spectroscopy (ATR-FTIR)

ATR-FTIR spectra were recorded using a Thermo Scientific Nicolet 6700 spectrophotometer using diamond tip in the range of 4000-600 cm^{-1}.

Nuclear Magnetic Resonance Spectoscopy (NMR)

^{13}C NMR spectrum in solution were recorded on a BrukerAvance 500 spectrometer equipped with a 5 mm triple resonanceinverse Z-gradient probe (TBI ^{1}H, ^{31}P, BB). Chemical shifts (δ, parts per million) are quoted by internal referencing to the ^{13}C residual signal of the deuterated solvent (THF-d_8).

Wide-Angle X-Ray Scattering (WAXS)

To obtain the diffractograms, an Empyrean Serie 3 diffractometer from Malvern Panalytical, equipped with a focusing mirror and a Galipix3D detector, was used. The radiation source used was that produced by a molybdenum anticathode $\lambda K\alpha$=0.071 nm). The samples were mounted in 0.5 mm glass capillaries, and the measurements were carried out in transmission geometry, with an angle range of 3 to 140° in 2° and an angular step of 0.03°.

X-Ray Photoelectron Spectroscopy (XPS)

XPS measurements are recorded on a Thermo Electron Kα spectrometer with a base pressure of 5×10^{-9} mbars. For high-resolution spectra, a pass energy of 20 eV is used and charging effect is neutralized with a dual e^{-}/Ar^{+} source. The C1s core peak of adventitious carbon at 285.0 eV is used as an internal energy reference. The data are treated with Casaxps using Gaussian–Lorentzian combinations for the fits and Scofield photoionization cross-section,[1] corrected for the analysis depth and the analyzer's transmission function, for quantification.

Magnetic measurement (VSM)

The magnetic properties of the nanoparticles were characterized, in powder state, using a Physical Property Measurement System (PPMS, Quantum Design) in the Vibrating Sample Magnetometer configuration (VSM). The temperature evolution of the magnetization under different field (μ_0H_{app} = 10 mT; 100mT; 1T and 5T) was recorded following the classical Zero-Field Cooling (ZFC)/Field Cooling (FC) measurements. Briefly the sample is cooled down from 300 K to 5 K in absence of any applied field (corresponding to the ZFC), then the external field is applied and the magnetization recorded during the temperature ramping from 5 K to 300 K, with a rate of 2 K/min. The sample is then cooled down to 5 K under the external field (FC). The magnetization is finally recorded during the temperature ramping from 5 K to 300 K, with the same rate of 2 K/min. To avoid any problem of remanence during the procedure, the ZFC/FC were performed with increasing field starting from the lowest one (10 mT). The susceptibility is deduced from the magnetization curve by: $\chi = \frac{M}{H}$ (Eq. 1)

Thermoremanence as a function of T was probed in zero field upon warming from 5K to 300K after the sample being field cooled under μ_0H = 9 T. ± 9 T hysteresis measurements were recorded at 300 K and 5 K after field cooling at 9 T. The dimensionless susceptibility is calculated by dividing the magnetization, expressed in A/m, by the magnetic field applied, also expressed in A/m. For that, the magnetic induction μ_0H expressed in tesla is converted following the relation:

1T -> 796 x 10^3 A/m

The magnetization, expressed in Am^2/kg is converted to A/m by considering the density of α-Mn (ρ = 7400 kg/m^3) : M(A/m) = M($A.m^2/kg$) x ρ (kg/m^3) (Eq. 2)

To avoid any oxidation, Teflon capsules were filled up with ~10mg of powder in the glove box, under an Ar atmosphere and then transferred to the VSM in a sealed container. After a first characterization in these conditions, the HDA-coated Mn nanoparticles were intentionally exposed to air by exposing the capsule 7 days under ambient conditions and the whole characterization set was repeated.

2. Synthesis and characterization data of Mn(mesityl)$_2$

The synthesis of the Mn precursor was adapted from a previously reported method with some modifications.[2–4] Diethyl ether (Et_2O) was employed instead of tetrahydrofuran (THF) to yield a coordinatively unsaturated Mn complex, denoted as **Mn(mesityl)$_2$**. First, bromo(mesityl)magnesium was synthesized in a round bottom flask by the addition of bromomesitylene (15.4 mL, 9.8 mmol) to a suspension of Mg turnings (3.6 g, 14.8 mmol) in Et_2O (80 mL) and refluxed for 4 h under inert atmosphere. The reaction is cooled down and filtered off via cannula obtaining an orange solution of ca 0.9 M.

In a Schlenk line, the bromo(mesityl)magnesium was added dropwise to a suspension of $MnCl_2$ (3 g, 23.8 mmol) in Et_2O (40 mL) under vigorous stirring at -78 ºC. After the addition, the reaction was heated up to room temperature and stirred for 18 h. Afterwards, the mixture was refluxed for 5 h. Then, dioxane (25 mL) was added in order to favor the precipitation of magnesium salts and the reaction was stirred for another 18 h. After that, the suspension was centrifugated (25000 rpm, 5 ºC, 25 min) and the brownish supernatant was transferred into a Schlenk and the volatiles components were removed under vacuum until dryness. The remaining solid was dissolved in Et_2O (75 mL) and kept in the freezer for 2 days allowing the crystallization of a beige powder which was isolated and dry under vacuum. The Mn complex was obtained as a beige solid with a yield of 75%. ^{1}H-NMR did not reveal any signal due to the paramagnetism of the complex (Figure S1).

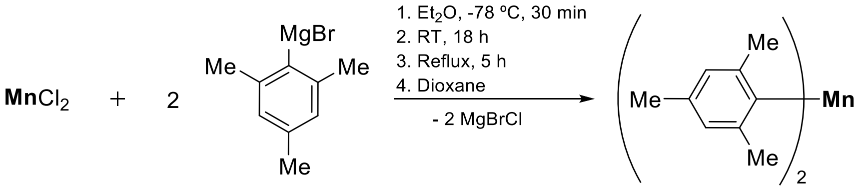

Scheme S1. Synthesis of Mn(mesityl)$_2$.

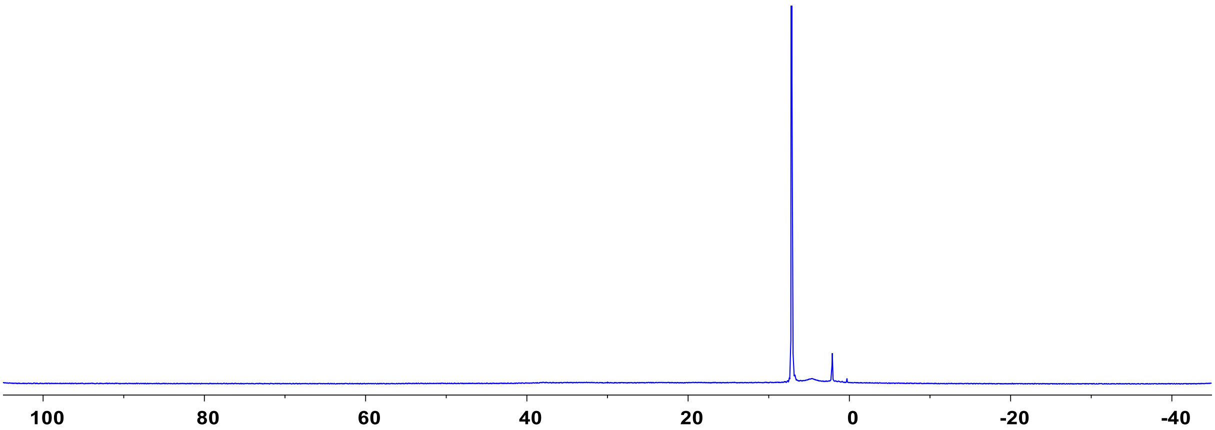

Figure S1. ^{1}H-NMR of Mn(Mesityl)$_2$ in benzene-d$_6$ (500 MHz, 298 K).

3. Synthesis of Mn nanoparticles

All the nanoparticles were synthesized using **Mn(mesityl)$_2$** as precursor following the organometallic approach method described by Chaudret et al.[5] The synthesis processes were carried out inside the glove box and under inert atmosphere in Fisher Porter bottles, previously placed in an oven for a minimum of 24 hours. Mn nanoparticles were synthesized by the addition of different ligands as stabilizers.

Mn@PA: Mn(mesityl)$_2$ (100 mg, 0.341 mmol) was placed into a 100 mL Fisher Porter bottle, followed by the addition of 3 mL of toluene. A suspension of palmitic acid (0.010, 0.017, 0.034 or 0.068 mmol) in 3 mL of toluene was introduced into the Fisher Porter. Subsequently, the system was pressurized with 3 bars of H_2 and immersed in a pre-heated silicon bath at 150 °C for 24 hours. Later, the Fisher Porter was carefully removed from the bath and allowed to cool down to room temperature. The resulting black solution was then subjected to centrifugation with acetonitrile (12 mL) for 5 minutes at 25.000 rpm and at 5 °C. The black NPs were dried under vacuum for 4 h and storage inside the glovebox.

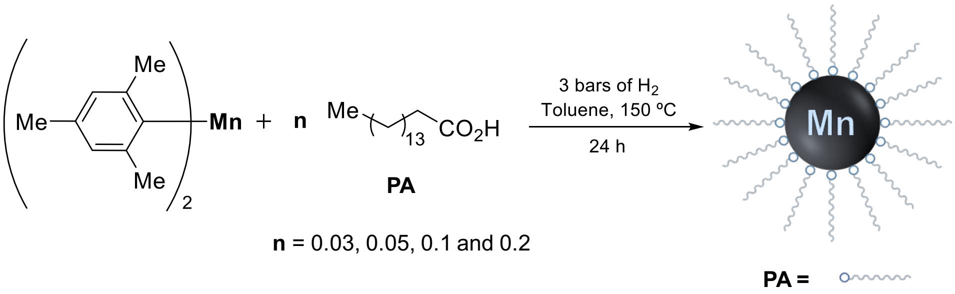

Scheme S2. Synthesis of **Mn@PA**

Mn@HDA: Mn NPs stabilized by HDA were synthesized following the same procedure previously described for **Mn@PA** with 0.033 eq (0.011 mmol, 2.7 mg), 0.5 eq (0.170 mmol, 41.2 mg) or 2.5 eq (0.852 mmol, 205 mg) of HDA.

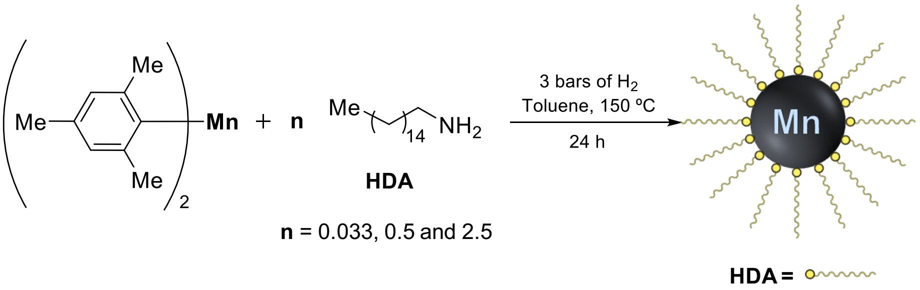

Scheme S3. Synthesis of **Mn@HDA**

Mn@DDA and **Mn@ODA**: Mn NPs stabilized by Octadecylamine (ODA) and Dodecylamine (DDA) were synthesized following the same procedure previously described for **Mn@PA** using 0.5 eq. of stabilizer: ODA (4.6 mg, 0.170 mmol), and DDA (3.1 mg, 0.170 mmol).

Mn@DMEDA, Mn@TMEDA, Mn@HMEDA: Mn NPs stabilized by different diamines were synthesized following the same procedure previously described for **Mn@PA**, using 0.25 eq. of stabilizer. The diamines used were: Dodecamethylenediamine (DMEDA, 17.1 mg, 0.086 mmol), Tetramethylethylenediamine (TMDA, 9.9 mg, 0.086 mmol), and1,6-hexanediamine (HMDA, 10.0 mg, 0.086 mmol).

Mn@HDA/PA: Mn NPs stabilized by HDA and PA were synthesized following the same procedure previously mentioned for **Mn@PA**, using 0.3 eq for HDA (36.7 mg, 0.15 mmol) and 0.03 eq. for PA (3.9 mg, 0.02 mmol).

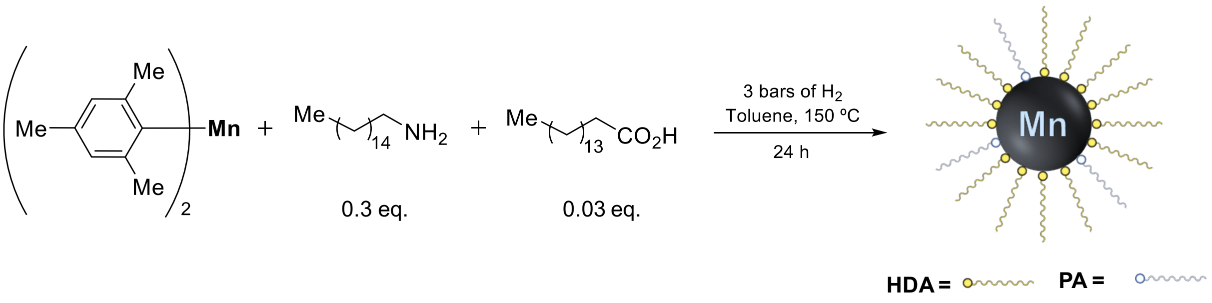

Scheme S4. Synthesis of **Mn@HDA/PA** NPs.

4. TEM images of Mn NPs

TEM pictures for the synthesis with PA

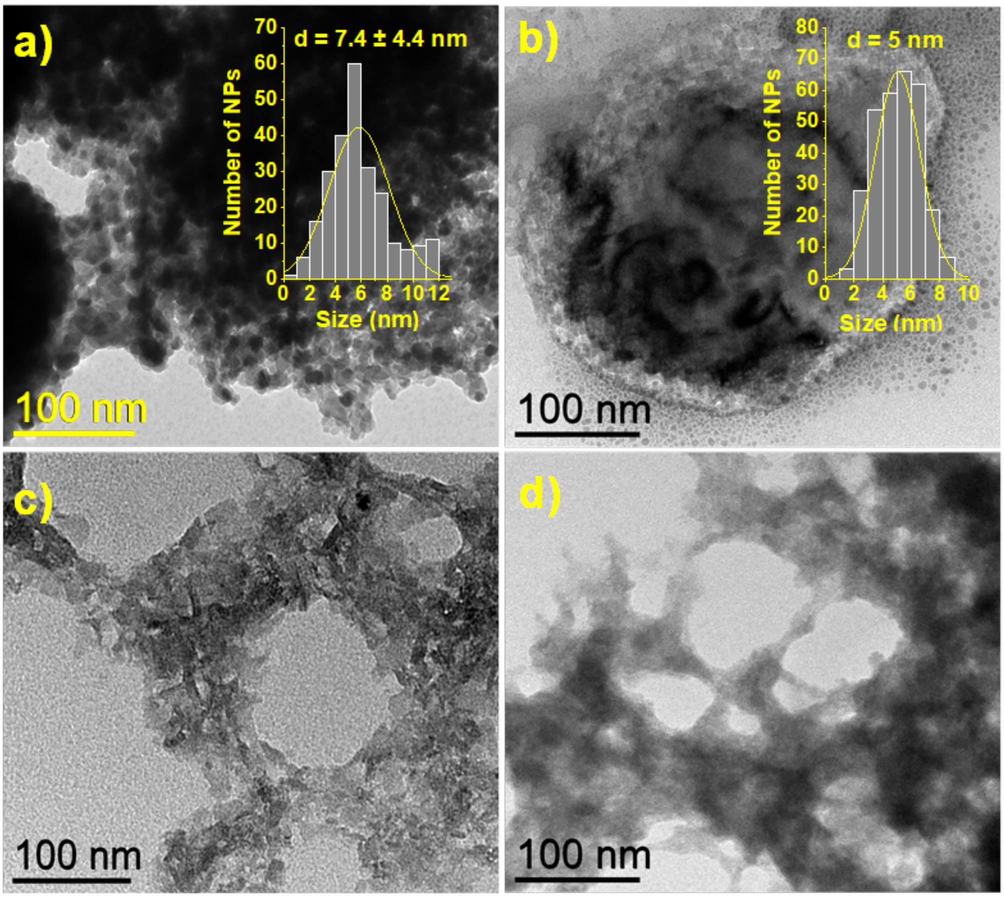

Figure S2. TEM micrograph of Mn@PA NPs using: a) 0.03 eq. (inset: size distribution) b) 0.05 eq. (inset: size distribution c) 0.1eq., and equiv d) 0.2 eq.

Table S1. Size of **Mn@PA** NPs.

Entry	PA Eq.	Size (nm)[a]
1	0.03	7.5 ± 4.4[b]
2	0.05	5 nm ± 1.5
3	0.1	-
4	0.2	-

[a] In all the samples agglomerated regions were observed.

[b] Counts of isolated nanoparticles in the sample. Larger NPs (d ~ 35 nm) were also observed

TEM pictures for the synthesis with HDA

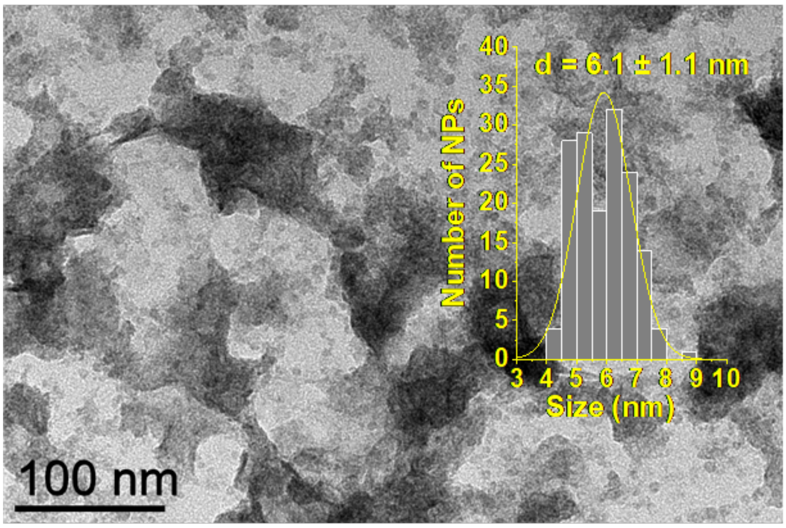

Figure S3. TEM micrograph of Mn@HDA NPs using 0.033 eq. of HDA.

Table S2. Size of **Mn@HDA** NPs with different concentration of HDA.

Entry	Ligand Equivalent HDA	Size (nm)
1	0.033	6.1 ± 1.1
2	0.5	5.2 ± 0.9
3	2.5	Not observed NPs

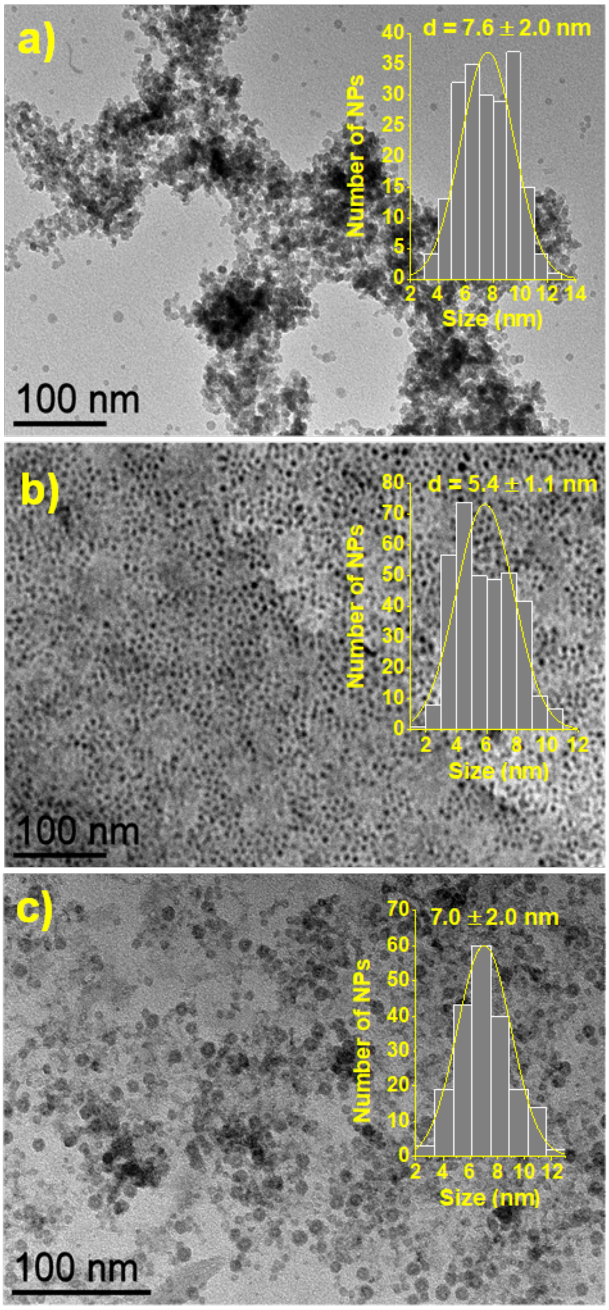

Figure S4. TEM micrograph of Mn NPs stabilized with 0.5 eq. of: a) DDO (inset: size distribution), b) HDA (inset: size distribution), and c) ODA (inset: size distribution).

Table S3. Size of **Mn@HDA, Mn@DDA and Mn@ODA** NPs.

Entry	Stabilizer	Size (nm)
1	DDO	7.6 ± 2.0
2	HDA	5.4 ± 1.1
3	ODA	7.0 ± 2.0

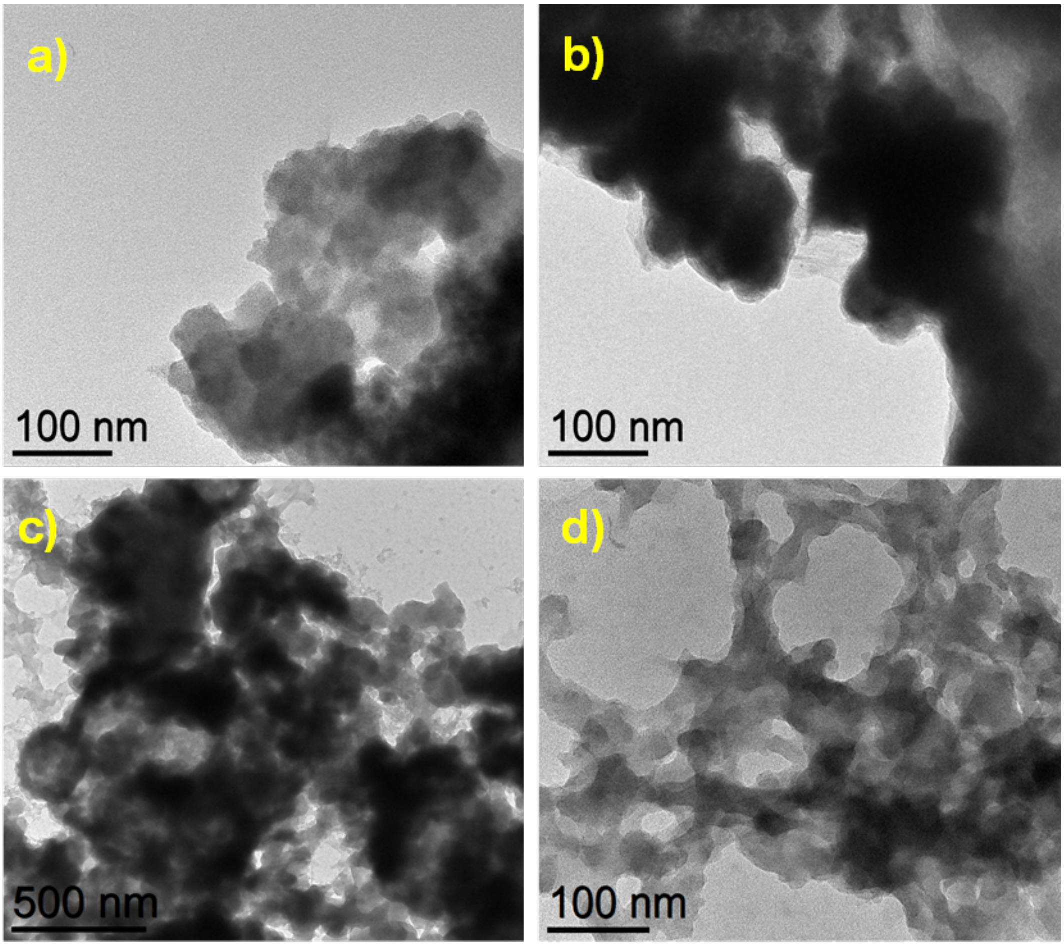

Figure S5. TEM micrograph of **Mn@diamine** NPs synthetized with 0.5 eq: a) Dodecamethylenediamine (DMEDA), b) Tetramethylethylenediamine (TMEDA), and c and d) 1,6-diaminohexane (HMEDA).

Table S4. Size of **Mn@diamine** using different diamines as stabilizing agent.

Entry	**Diamine**	**Size (nm)**
1	DMEDA	Agglomerates
2	TMEDA	Agglomerates
3	HMEDA	Agglomerates

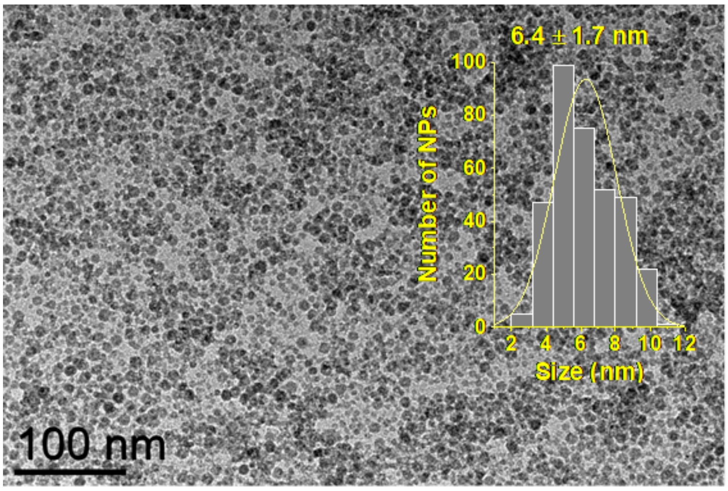

Figure S6. TEM micrograph (inset: size distribution) of Mn@HDA/PA (0.3:0.03) NPs.

Table S5. Size of **Mn@HDA/PA** NPs with different HDA/PA proportions.

Entry	**HDA:PA**	**Size (nm)**
1	0.3:0.03	6.4 ± 1.7
2	1.0:0.1	Agglomerates

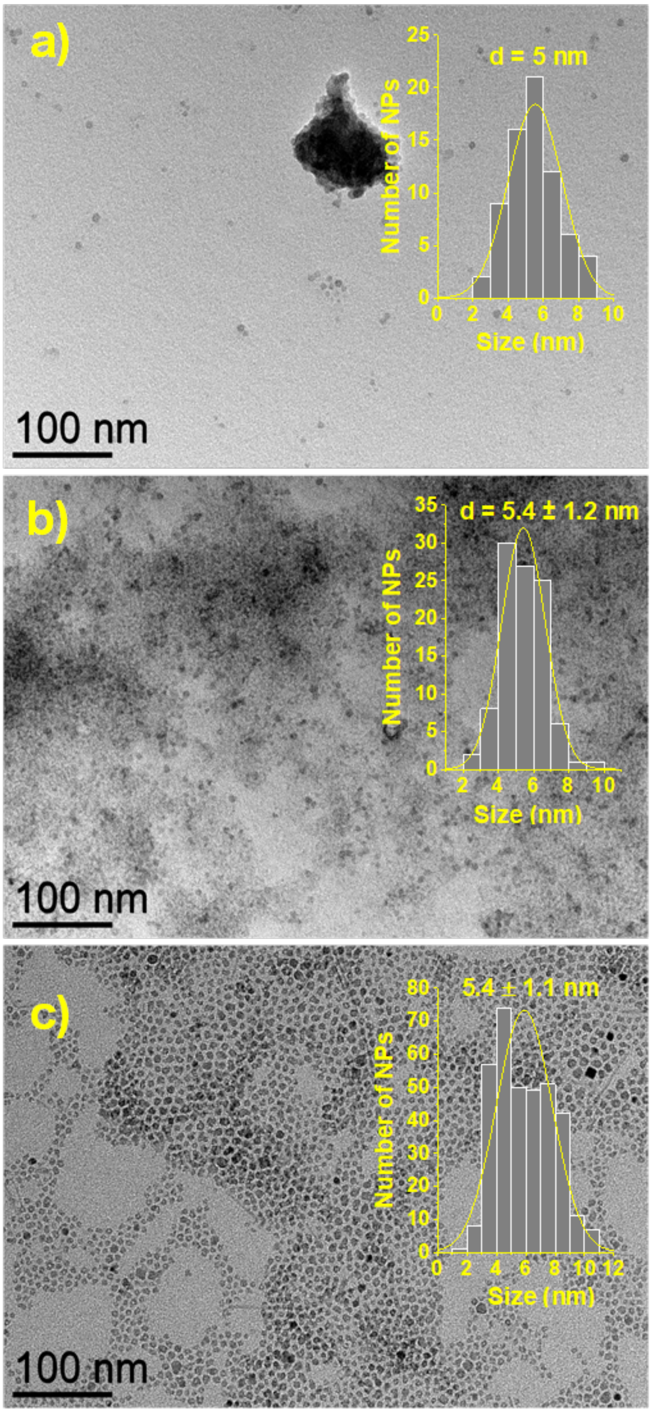

Figure S7. TEM micrograph of Mn@HDA NPs synthetized using 0.5 eq. of HDA at different temperatures a) 100 °C b) 125 °C c) 150 °C.

Table S6. Size of **Mn@HDA** NPs using 0.5 eq. of HDA at different temperatures.

Entry	**Temperature (° C)**	**Size (nm)**
1	100	5 ± 1.5[a]
2	125	5.4 ± 1.1[a]
3	150	5.4 ± 1.1

[a] Samples with agglomerated regions

6. IR measurements for Mn NPs

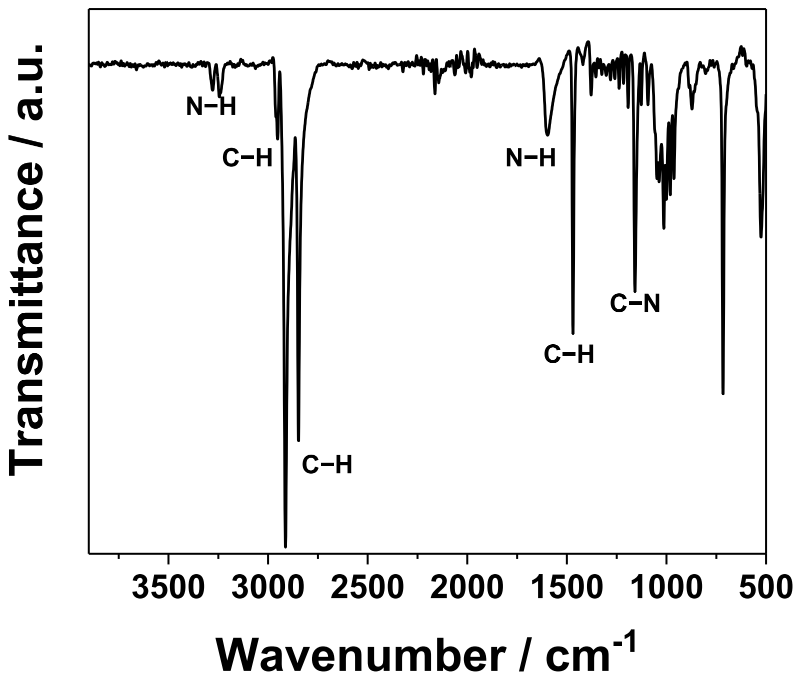

Figure S8. IR spectrum of the as prepared Mn@HDA NPs.

7. NMR measurements for Mn NPs

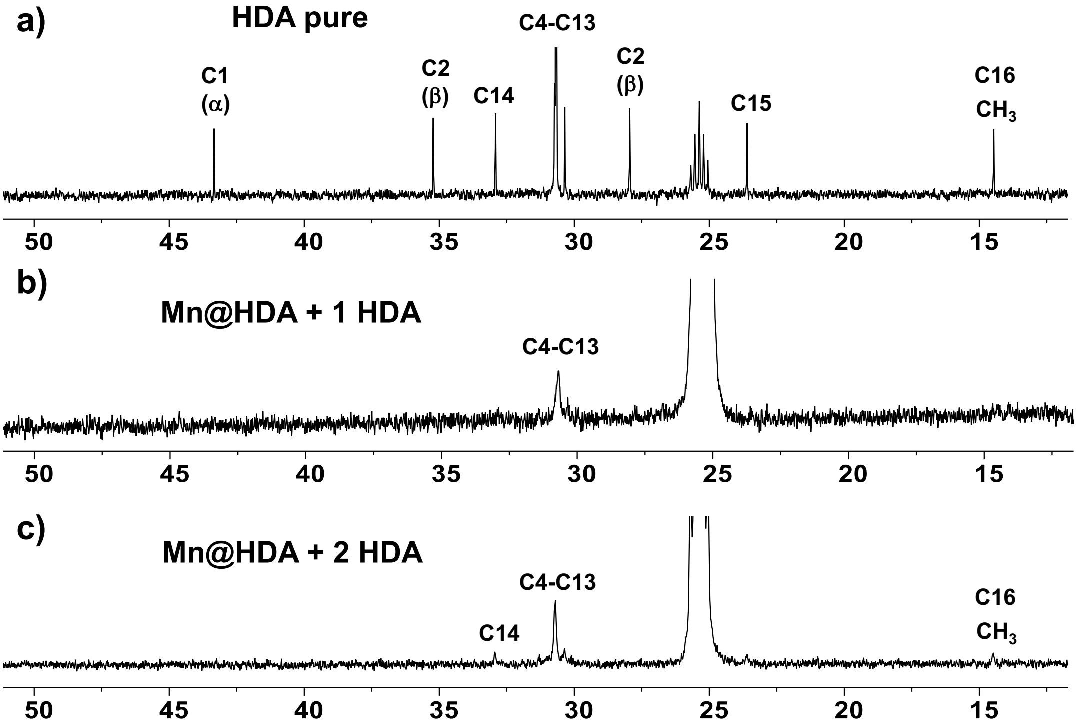

Figure S9. $^{13}C\{^1H\}$-NMR in thf-*d₈* (101 MHz, 298 K) spectra of a) commercial HDA, b) Mn@HDA with 1 equiv. of HDA, and c) **Mn@HDA** with 2 equiv. of HDA.

5. TGA of Mn NPs

TGA were carried out in order to determine the metal content in **Mn@HDA** and **Mn@HDA/PA**. The analysis was performed using a temperature program with two steps: the first one is the oxidation in air of the sample and is, then, followed by reduction to recover solely the metal. For **Mn@HDA**, the metal content was found to be 36% (matching the theorical Mn content: 31.3%) while for **Mn@HDA/PA**, a slightly higher the metal content was observed 48% (theorical Mn content: 38%).

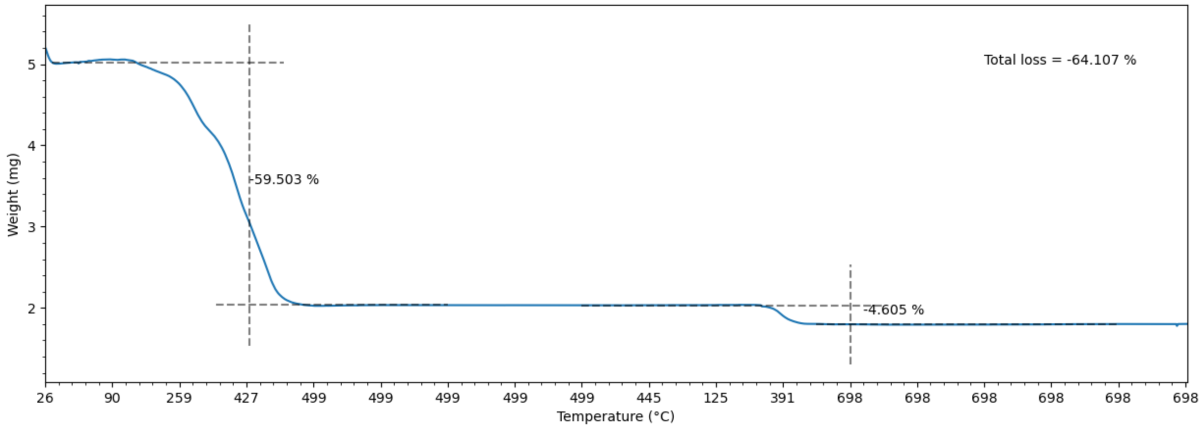

Figure S10. TGA profiles of **Mn@HDA** (0.5 eq. HDA) NPs.

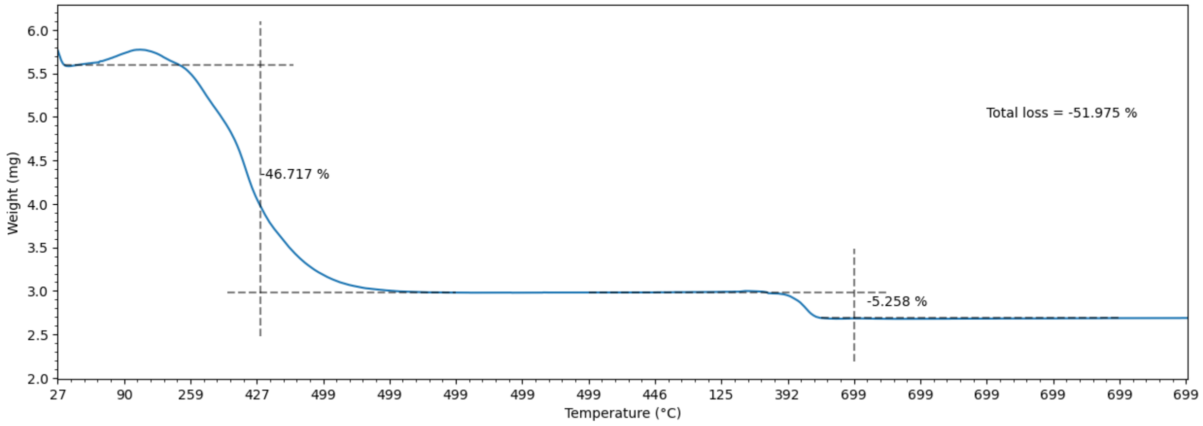

Figure S11. TGA profiles of **Mn@HDA/PA** (0.3:0.03) NPs.

8. XRD measurements of Mn NPs

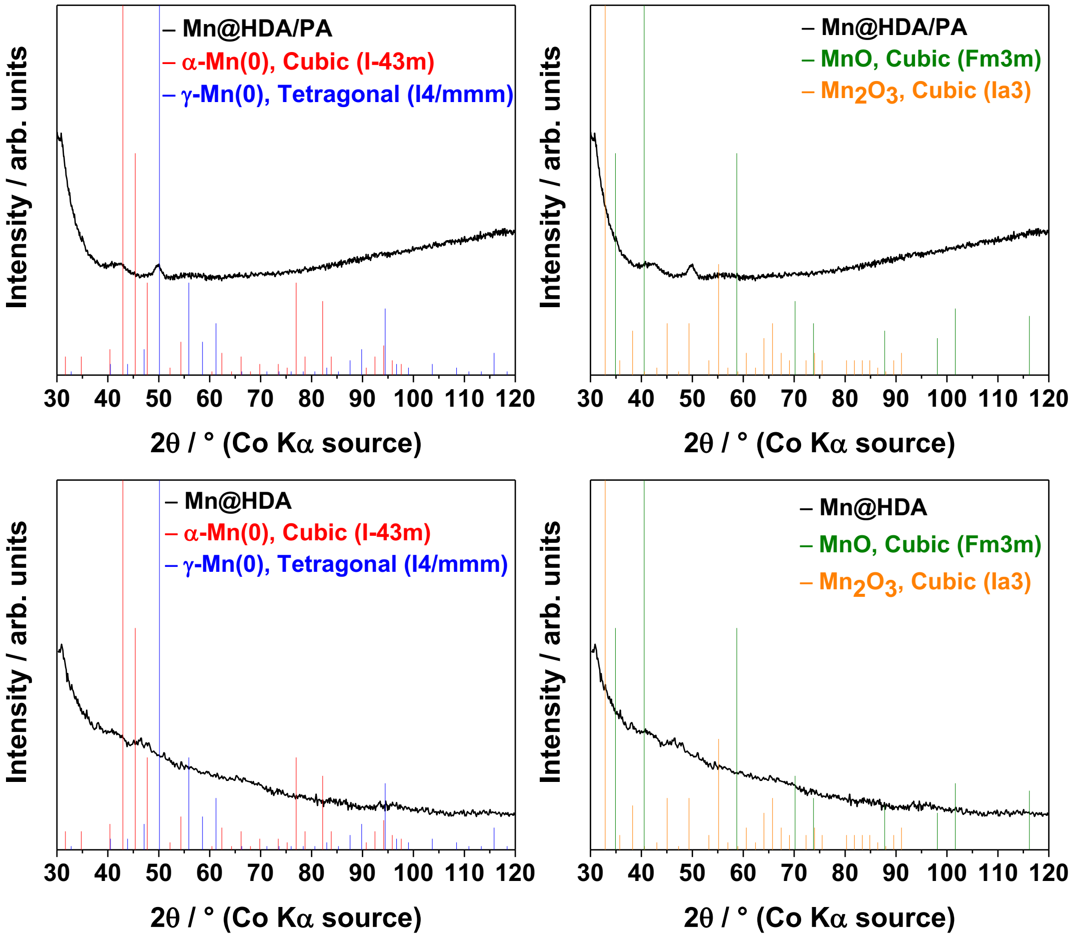

Figure S12. Diffractograms of Mn@HDA (0.5 eq. HDA) NPs with peaks corresponding to a) Mn(0) α and γ[5] and b) manganese oxides (MnO and Mn$_2$O$_3$),[6] and Mn@HDA/PA (0.3:0.03) NPs with c) peaks of Mn(0) α and γ, and d) peaks of manganese oxides (MnO and Mn$_2$O$_3$).

9. HR-TEM images for Mn NPs.

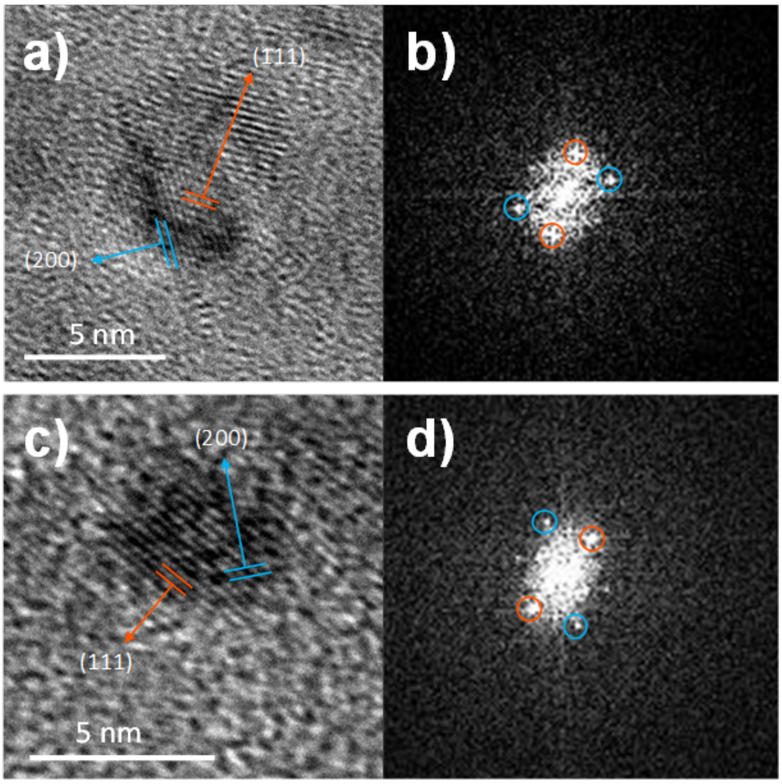

Figure S13. a) and c) HR-TEM micrograph of Mn@HDA (0.5 eq HDA) and assignment of crystallographic planes and b) and d) their FFT analysis without air exposure.

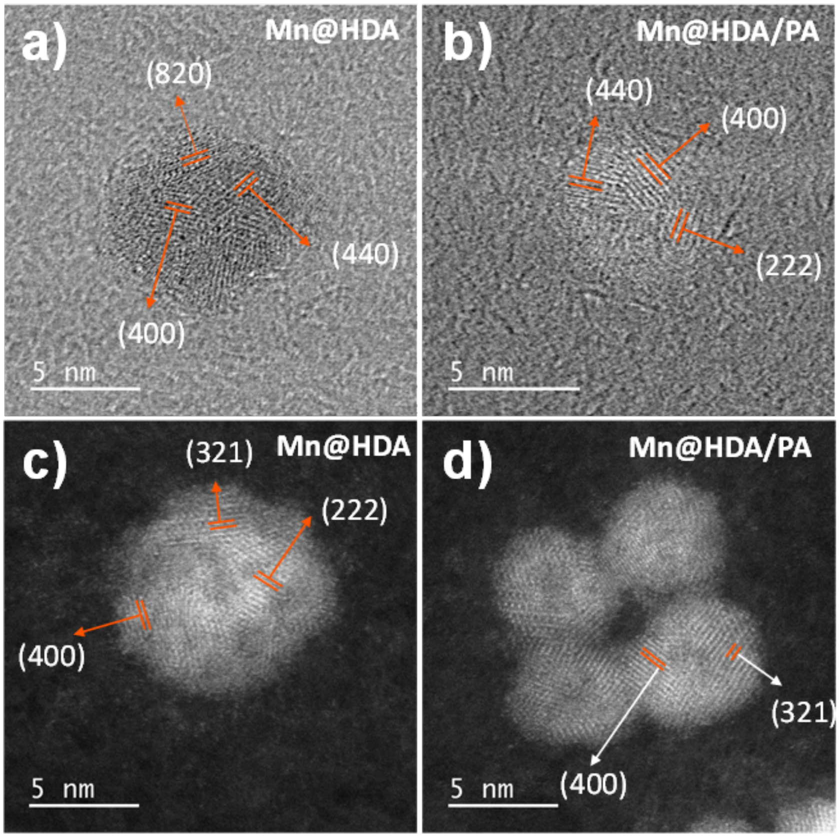

Figure S14. HR-TEM micrograph of a) Mn@HDA (0.5 eq. HDA) NPs and b) Mn@HDA/PA (0.3:0.03) and HR-HAADF c) Mn@HDA (0.5 eq. HDA) NPs and c) Mn@HDA/PA (0.3:0.03) with air exposure and assignment of crystallographic planes.

Angle calculation of Mn(0)

In order to calculate the angle between the crystallographic planes (200) and (111) of MnO, we used:

$$\vec{a} \cdot \vec{b} = x_A x_B + y_A y_B + z_A z_B = \|\vec{a}\| \|\vec{b}\| \cos\theta$$

So:

$$2 = 2\sqrt{3}\cos\theta$$
$$\theta = 54°$$

Angle calculation of α-Mn

With the same formula we obtain an angle between the planes (220) and (211) of 30°

10.WAXS of Mn NPs.

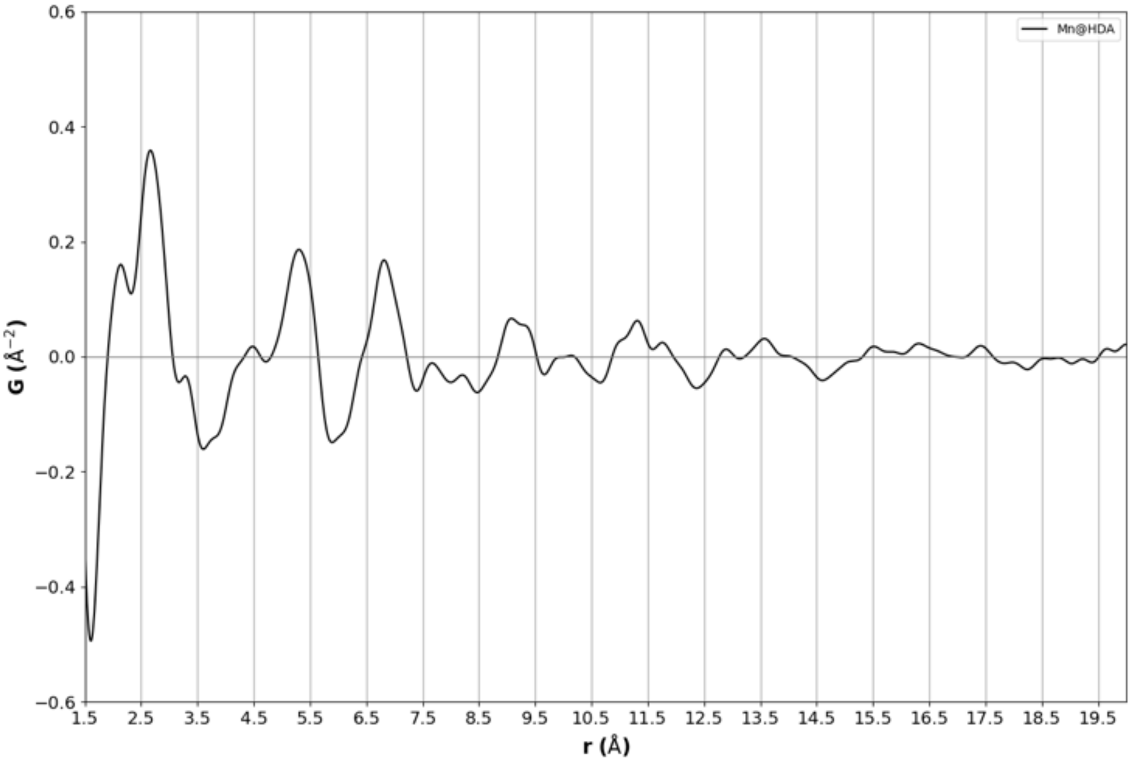

Figure S15. Pair distribution function (PDF) obtained for Mn@HDA (0.5 eq. HDA) NPs.

Table S7. Comparison between the distances obtained with Mn@HDA (0.5 eq. HDA) NPs and the theoretical distances of the various possible species

Sample	Mn_2O_3	α-Mn	β-Mn	MnO
2.15	1.97	2.65	2.63	2.24
2.68	2.27	3.65	3.15	3.13
3.31	3.12	4.14	3.51	3.91
4.46	3.65	4.65	3.98	4.42
5.37	4.76	5.14	4.52	4.94
6.82	5.75	6.09	5.12	5.43
9.08	6.17	6.65	6.37	6.24
9.32	7.17		6.79	6.69
	8.8			

11.XPS measurements for Mn NPs

The XPS spectrum of Mn@HDA recorded in the Mn 2p energy is very similar to that of the Mn(0) prepared by Köppler et al.[7] (Figure S16) and consists of two main peaks. The first one located at 639.5 eV lies in the region which is characteristic of the Mn 2p energy of zero-valent Mn. Then, a second intense peak at 642.3 eV is attributed to Mn species with an oxidation number of +2 corresponding to surface Mn atoms: on one hand, this concerns those interacting with HDA ligand and on the other hand, to Mn atoms oxidized because of the brief exposure to air during the introduction of the sample. Again, this assignment is consistent with Köppler's results who assigned the corresponding peak to the outermost Mn atoms which interact with the ligands bearing electronegative atoms. In order to confirm unambiguously the assign of the peak at 639.5 eV to Mn(0), we analyzed this sample after air exposure (Mn@HDA-Ox2) following the same strategy than that Köppler et al. (Figure S17). As expected the peak at 639.5 eV of Mn(0) disappears. Interestingly, the Mn 3s spectrum can also be of interest in order to identify the different type of oxide: it displays a doublet whose splitting value of 5.5 eV is characteristic of Mn^{3+} oxidation thus suggesting that oxidation yields to Mn_2O_3.

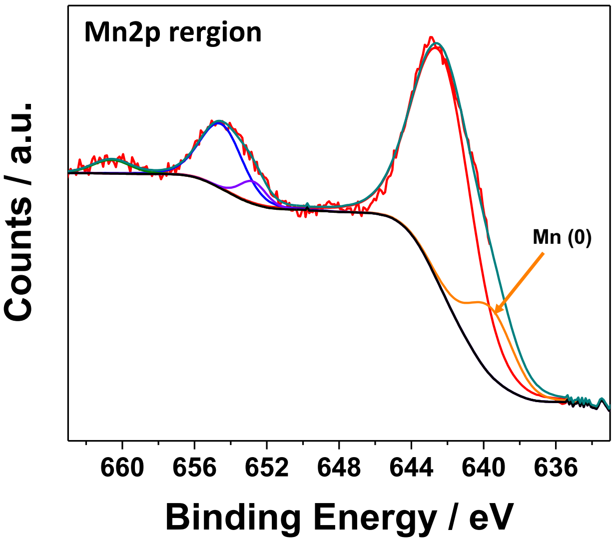

Figure S16. XPS spectra of the Mn2p region for the as prepared **Mn@HDA** NPs.

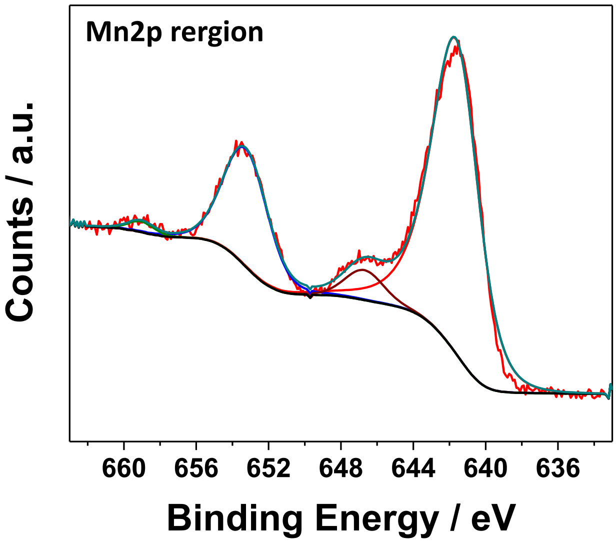

Figure S17. XPS spectra for Mn2p region for the oxidized **Mn@HDA** NPs.

12. Magnetic measurements of Mn NPs

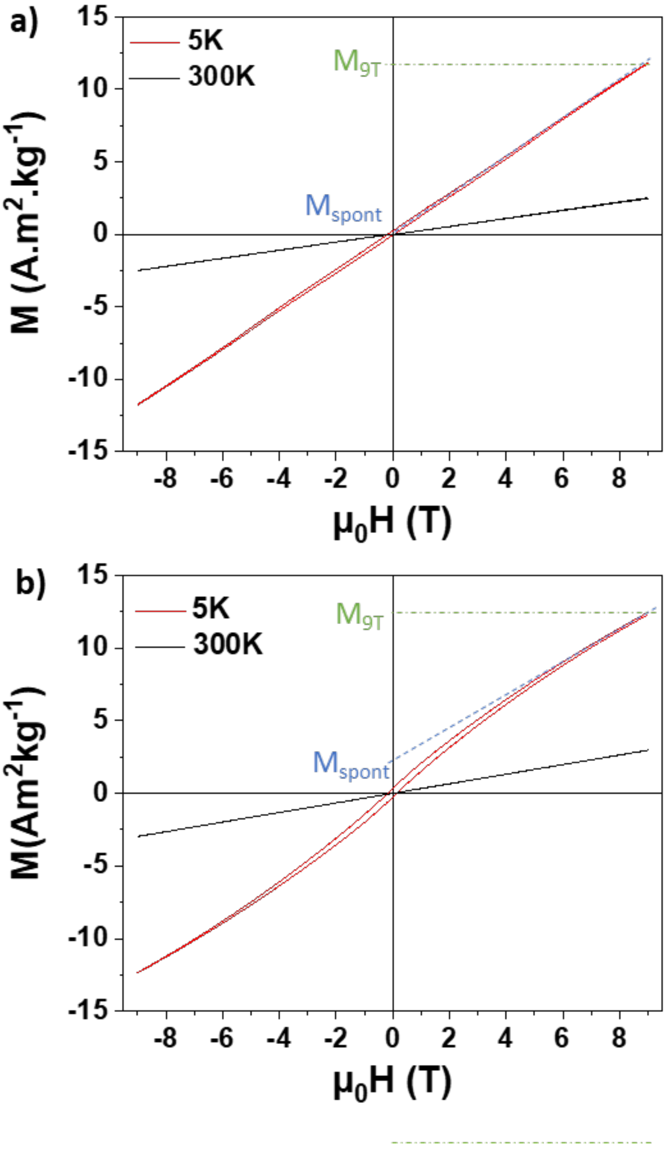

Figure S18. Magnetization measurements as a function of applied field recorded at 300K (black line) and 5K (red line) for a) Mn@HDA (0.5 eq. HDA) NPs and b) Mn@HDA-Ox2 after 7 days of air exposure. Dashed lines are guide to the eye for the spontaneous magnetization M_{spont} (blue) and the magnetization measured at 9T M_{9T} (green).

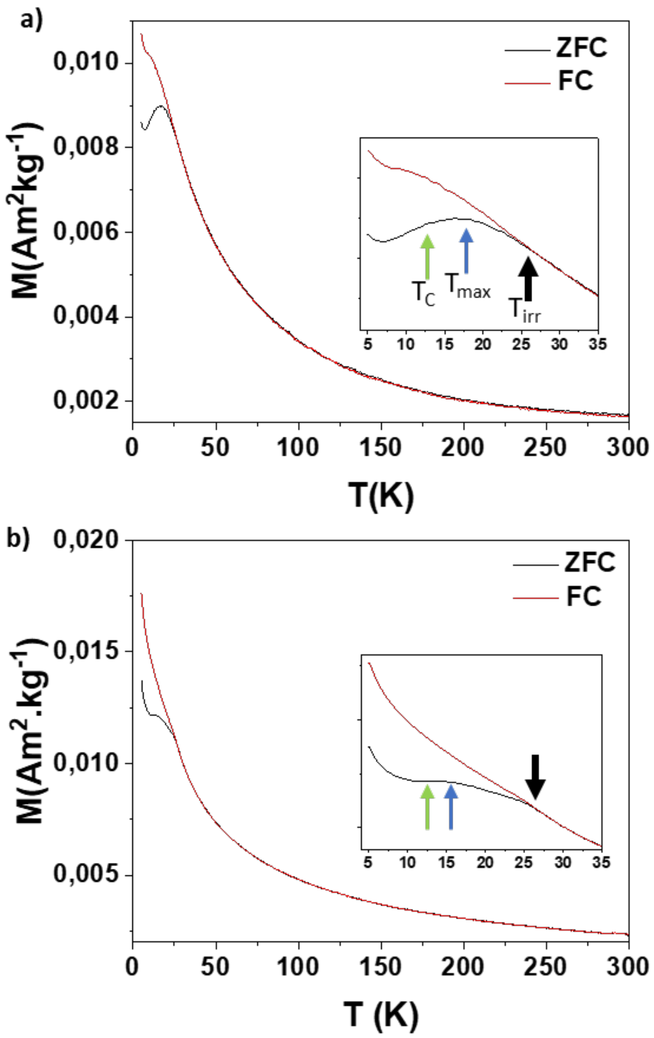

Figure S19. Evolution of the magnetization upon temperature increase after the sample was cooled under zero magnetic field (zero-field-cooled ZFC, black line) and under a 10 mT field (field-cooled FC, red line) for a) as prepared Mn@HDA (0.5 eq. HDA) and b) Mn@HDA-Ox2 after 7 days of air exposure. The arrows are guide to the eye for the critical temperature (T_c, green), the maximum peak temperature (T_{max}, blue) and the irreversible temperature (T_{irr}, black).

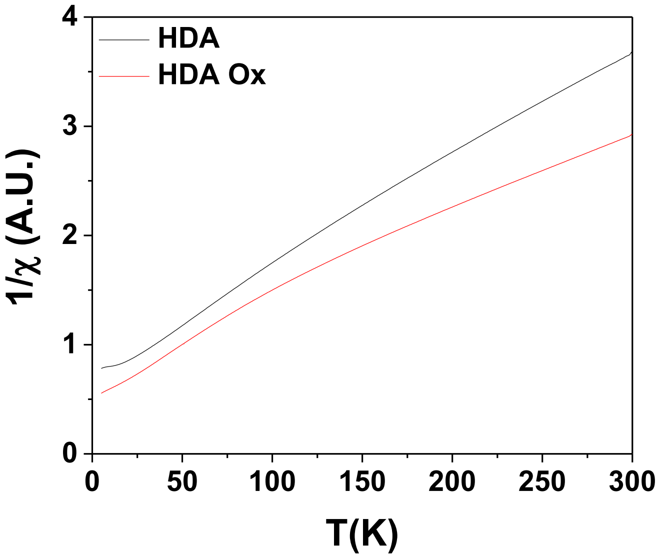

Figure S20. Temperature evolution of the inverse of the susceptibility measured at $\mu_0H = 5T$ on Mn@HDA (0.5 eq. HDA) without air exposure (black line) and after 7 days of air exposure (blue line), and Mn@HDA/PA (0.3:0.03) NPs (red line). The dashed lines are guide to the eye for the domain validity of the Curie-Weiss law which implies a linear dependence with temperature. In the case of the oxidized NPs, the domain is fairly restricted to high T (T> 200K).

13. Catalytic tests

GS-MS Method: The initial temperature, 35 °C, was hold for 5 min. Then, increased to 60 °C at 10 °C min^{-1}. Finally, increased to 150 °C at 10 °C min^{-1} and hold for 5 minutes. The injector temperature was settled at 250 °C and the carrier gas (hydrogen) flowed at 2 mL min^{-1}.

General procedure for the catalytic experiments: In a typical experiment, 0.65 mmol of substrate, 0.5 mmol of dodecane used as internal standard, and ca. 10 mg of Mn@HDA catalyst (10 mol % based on Mn content) were mixed in a 100 mL Fisher–Porter bottle in the glove box. The reactor was charged with 3 bars of H_2 and placed in a preheated oil bath (80 or 110 ºC) for 20 h. At the end of the reaction, the FP was cool down, and pressure was released. The catalyst was separated by filtration through an Alumina column. After that, 10 drops of the liquid were taken and diluted in 1.3 mL of dichloromethane for GC-MS analysis.

Selected Chromatograms after the Catalytic runs.

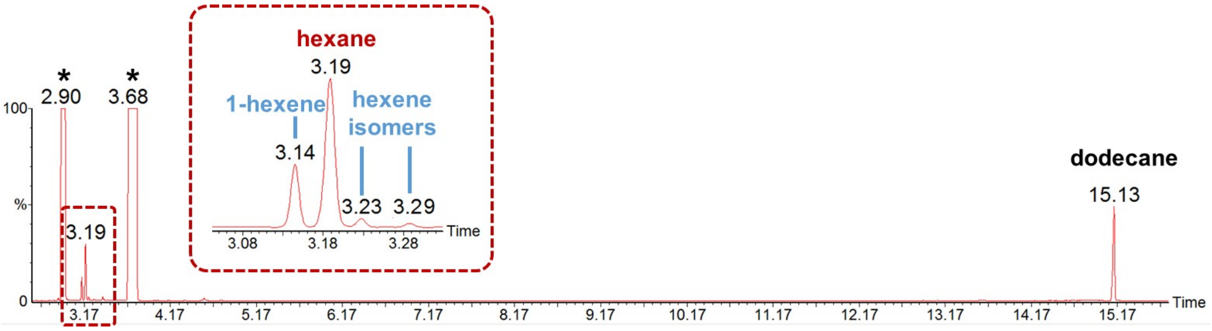

Figure S21. GC-FID Chromatogram after the hydrogenation of 1-hexene after 20 h at 80 ºC. Reaction conditions: 1-hexene (0.65 mmol), dodecane (Internal Standard, 0.5 mmol), 5 mL of cyclohexane, 80 ºC, 800 rpm, 20 h. The inset shows the region of the substrate (1-hexene) and the products (hexane and internal hexenes) of the reaction. The asterisks denote the peaks for the dilution solvent (dichloromethane at 2.90 min) and the reaction solvent (cyclohexane at 3.68 min).

14.Characterizaton after catalysis

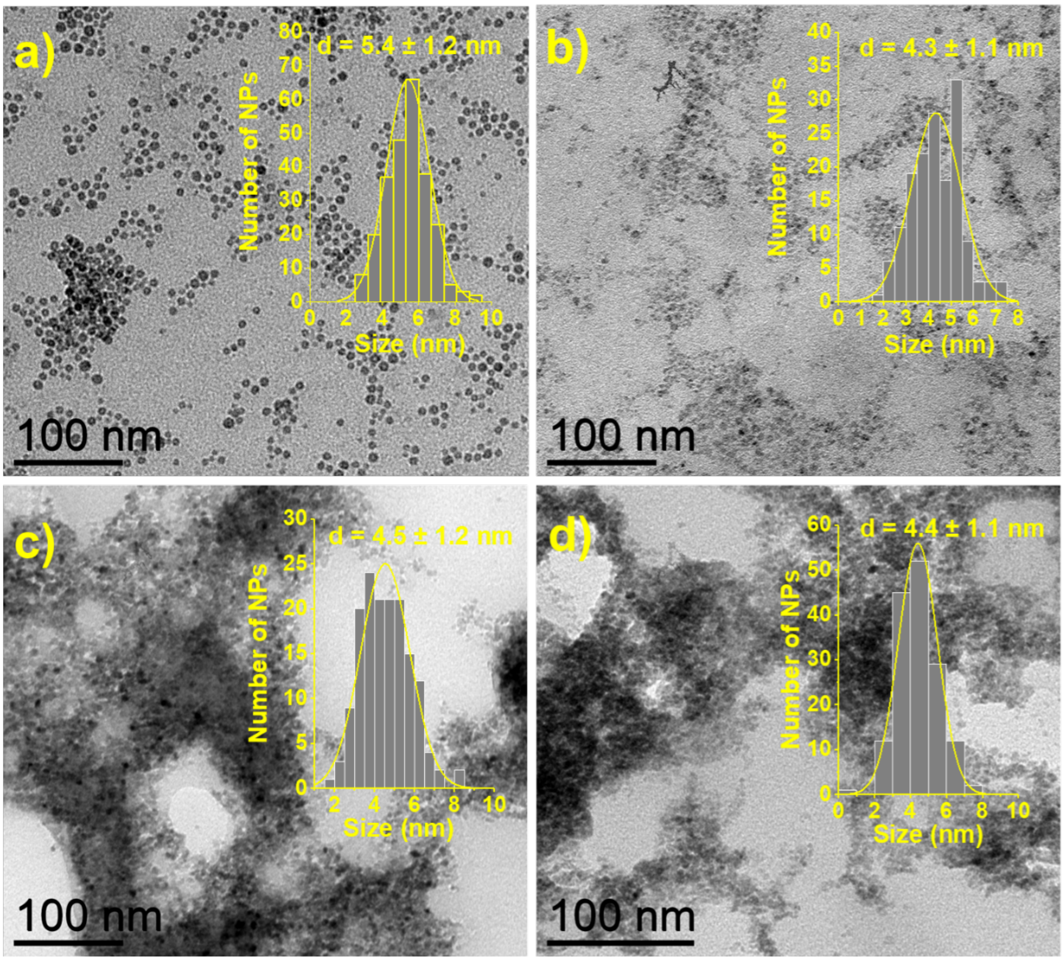

Figure S22. TEM micrographs (inset: size distribution) after catalytic run using a) 1-hexene, b) phenylacetylene, c) 2-butanone, and d) acetophenone.

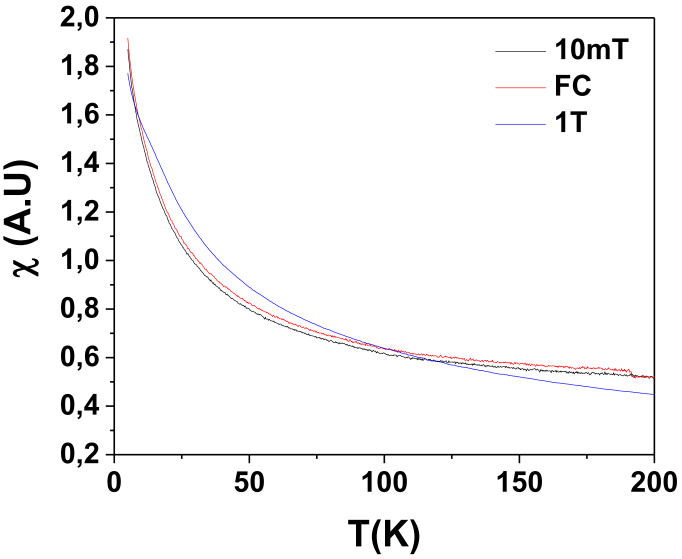

Figure S23. Evolution of the magnetization upon temperature increase under 1T (blue line) or 10 mT (black, red) after the sample was cooled under zero magnetic field (zero-field-cooled ZFC, black and blue lines) and under 10 mT (field-cooled FC, red line) of **Mn@HDA** after catalysis with 1-hexene.

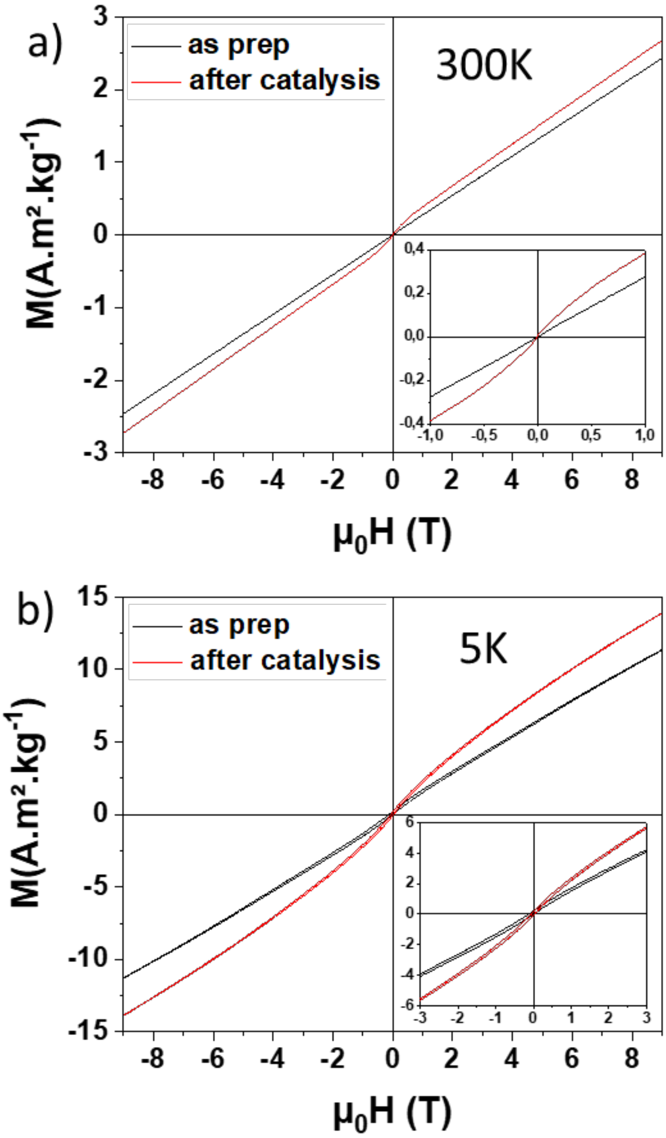

Figure S24. Magnetization measurements as a function of applied field recorded on HDA-Mn NPs as prepared (black line) and after catalysis with 1-hexene (red line) at a) 300K and b) 5K.

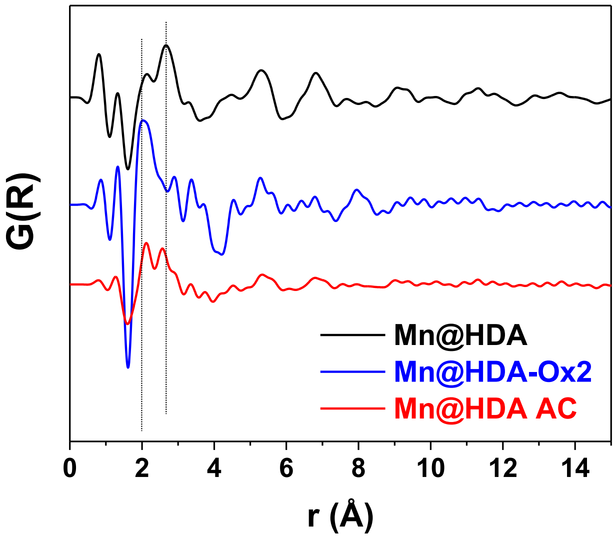

Figure S25. Pair Distribution Function obtained on as prepared, oxidized, and after catalysis Mn@HDA NPs.

15. References

1 J. H. Scofield, *J. Electron Spectrosc. Relat. Phen.*, 1976, **8**, 129–137.

2 E. Solari, F. Musso, E. Gallo, C. Floriani, N. Re, A. Chiesi-Villa and C. Rizzoli, *Organometallics*, 1995, **14**, 2265–2276.

3 S. Gambarotta, C. Floriani, A. Chiesi-Villa and C. Guastini, *J. Chem. Soc., Chem. Commun.*, 1983, 1128.

4 R. Fischer, H. Görls, M. Friedrich and M. Westerhausen, *J. Organomet. Chem.*, 2009, **694**, 1107–1111.

5 C. Amiens, B. Chaudret, D. Ciuculescu-Pradines, V. Collière, K. Fajerwerg, P. Fau, M. Kahn, A. Maisonnat, K. Soulantica and K. Philippot, *New J. Chem.*, 2013, **37**, 3374.

6 H. E. Swanson, M. I. Cook, T. Isaacs and E. H. Evans, *Standard X-ray Diffraction Powder Patterns*, Washington, D.C., 1960, vol. 9.

7 R. Franke, J. Rothe, R. Becker, J. Pollmann, J. Hormes, H. Bönnemann, W. Brijoux and R. Köppler, *Adv. Mater.*, 1998, **10**, 126–132.